Polymer rigidification in graphene based nanocomposites: Gas barrier effects and free volume reduction

David Roilo [a, *], Pushkar N. Patil [a, **], Roberto S. Brusa [a], Antonio Miotello [a], Stefano Aghion [b], Rafael Ferragut [b], Riccardo Checchetto [a]

[a] *Department of Physics, University of Trento, via Sommarive 14, I-38123 Povo, Trento, Italy*
[b] *Department of Physics and L-NESS, Politecnico di Milano, via Anzani 42, I-22100 Como, Italy*

The gas transport properties of polymer nanocomposite membranes made of Few Layer Graphene nanoplatelets dispersed in amine-modified epoxy resins were studied by gas phase permeation analysis with H_2, N_2 and CO_2. The gas permeability of the nanocomposites decreases with increasing filler content. Filler addition does not change the gas selectivity of the pure epoxy membrane. Positron Annihilation Lifetime Spectroscopy analysis indicates that, by increasing the filler content, the free volume structure does not change but the fractional free volume decreases. Gas transport results were explained by the formation of a constrained polymer region of thickness l_{if} at the filler-matrix interface. The l_{if} parameter was evaluated from the reduction of the fractional free volume of the nanocomposite samples with respect to that of the epoxy matrix. The average value of l_{if}, ~ 20 nm, permits to reproduce quantitatively the experimental data at all examined temperatures, filler concentration and test gas.

1. Introduction

Polymer nanocomposites containing gas-impermeable, high aspect ratio nano-particles (such as silicate clays) are of great interest for the packaging technology because they have demonstrated the potential to overcome the gas barrier performances of commercial polymer films [1]. Graphene and graphene-derived nanomaterials are attracting particular attention because the resulting polymer nanocomposites, in addition to the improved gas barrier performances [2], also show enhanced mechanical, thermal and electrical properties [3].

Experimental results on the gas transport properties of this class of polymer nanocomposites are generally discussed by assuming that the continuous polymer phase completely wets the filler particles and no chemical or physical interaction exists between the polymer chains and the filler surface [4]. According to this assumption, the polymer layers at the filler-matrix interface maintain the same structure and gas transport properties as in the bulk polymer: the permeability of the nanocomposite thus results lower than that of the matrix because the filler particles force the penetrant molecules to travel along more tortuous and longer diffusion paths [5]. Models consider how the filler particle properties (aspect ratio), the nanocomposite structure (volume fraction occupied by the filler particles, filler dispersion degree, orientation and texture) or variations in the matrix crystalline degree influence the geometry of the diffusion path [2,6].

However, the different chemical and physical properties of the filler and matrix phases give rise to peculiar structural properties of the interfacial layers at the filler-matrix internal boundaries and to "non-ideal" effects in the gas transport properties of polymer nanocomposites [7,8]. When the polymer-filler interfacial adhesion is good, the free volume in the polymer layers near the filler surface decreases because thermal fluctuations of the polymer chains are reduced. This effect, which is called polymer rigidification, enhances the gas barrier performances of the nanocomposite because the rigidified polymer layers presents lower gas permeability than the pure polymer matrix [7,8]. On the opposite, the poor adhesion between the polymer and filler particles produces interface nanovoids: these defects increase the permeability of the nanocomposite acting as preferential and fast migration paths for the penetrant molecules [7,8].

The aim of this study is to obtain a deeper understanding of the

* Corresponding author.
** Corresponding author.
   E-*mail addresses:* david.roilo@unitn.it (D. Roilo), pushkhem6@gmail.com (P.N. Patil).

complex phenomena occurring at the filler-matrix interface in a graphene-based polymer nanocomposite as this is an important step for the successful development of innovative materials for packaging applications and gas separation processes [9]. Here we present a study evidencing that the filler-matrix interface layers control the gas transport properties of a model graphene-based polymer nanocomposite consisting of a blend of amine-modified epoxy resins with dispersed Few Layer Graphene (FLG) nano-platelets.

Amine-modified epoxy resins are cross-linked polymers that we have well characterized, as pure polymer membranes, in terms of gas transport properties and free volume structure [10,11]. FLG is a graphene-derived material which consists of a ordered stack of few graphene layers with total thickness in the 10 nm range and lateral size up to 0.1 mm [12,13]. The large aspect ratio and the wide surface area of the GNPs thus maximizes the filler-matrix interface area. We have prepared nano-composite membranes by systematically changing the filler content and studied the transport of penetrant molecules with different molecular sizes and condensation properties (namely H_2, N_2 and CO_2). The filler content was changed up to ~5 vol % to avoid nanoparticles agglomeration [13,14].

Structural information evidencing the formation of rigidified layers or of nano-sized voids were obtained by studying the free volume structure of the pure polymer and of the polymer nanocomposite samples by Positron Annihilation Lifetime Spectroscopy (PALS) [15,16]. A positron injected in a polymer matrix thermalizes and exists as "free" positron (e^+) with mean lifetime τ_2 of 0.3–0.5 ns or forms an electron-positron bound state called positronium (Ps). The singlet state is called para-positronium (p-Ps) and presents a mean lifetime τ_1 of 125 ps. The triplet state is called ortho-positronium (o-Ps) and presents a mean lifetime τ_3 of 142 ns in vacuum. In polymers, o-Ps is trapped in nanometer-sized regions of lower electron density (hole free volumes) such as voids: here it annihilates with a surrounding electron having opposite spin ("pick-off" mechanism) and its mean lifetime is consequently reduced to few ns. Therefore, in polymers the τ_3 value depends on the average size of the hole free volumes while the intensity I_3 of the signal related to the o-Ps annihilation depends on the number density of the holes [15,16].

2. Experimental section

2.1. Nanocomposites preparation

Expandable graphite flakes provided by Faima srl (Milan, Italy) were submitted to thermal shock (750 °C, 3 min) to obtain filaments of expanded graphite. Few Layer Graphene (FLG) nano-platelets were fabricated by submitting the filaments to ultra-sonic treatment in acetone (C_3H_6O) for 30 min at room tempera-ture. FLG powders were obtained by drying the resulting suspension in air. Details are reported in Ref. [17]. For the prepa-ration of the pure and the nanocomposite membranes we used NeoPentyl Glycol Diglycidyl Ether (NPGDE), having epoxy equiva-lent weight of 145 ± 5 g/eq (Sigma-Aldrich SRL, Italy) and a poly oxypropylene diamine as a cross-linking agent (Jeffamine ED-900, Huntsman Chemical Co.). FLGs powders were dispersed in acetone and the suspension was: i) first stirred for 30 min using a mechanical stirrer at 100 rpm and ii) then sonicated for 20 min using a horn sonicator. The desired amount of epoxide was then added to the solution, which was stirred again for 3 more hrs. and left overnight. The cross-linking agent was then added in stoi-chiometric ratio in order to achieve a 1:1 ratio between epoxy groups and amine hydrogens. The obtained solution was then stirred for 30 min and casted on a glass substrate. Pre-curing was

carried out at 50 °C for 4 h and post-curing at 80 °C for 12 h. For the present study we prepared pure and four nanocomposite membranes with 1, 5, 7.5 and 10 wt % filler content equivalent to 0.6, 2.8, 4.3 and 5.7 vol %, given the mass densities of 1.1 and 2.1 mg/mm^3 for matrix and filler, respectively. For more details regarding the preparation of the pure polymer sample, refer to our previous work [10].

2.2. Nanocomposite characterization

The structure of the pure polymer and of the nanocomposite membrane samples was studied by X-Rays Diffraction analysis (XRD). Measurements were done in Bragg-Brentano configuration using the Cu K$_\alpha$ radiation (λ = 1.54 Å) with XPert Pro Panalytical diffractometer. The morphology of the sample surface and of the sample cross-section was analyzed by Scanning Electron Microscopy (SEM) with a Field Emission JEOL JSM-7001F instrument. The cross-section was studied using membranes sandwiched between conductive scotch tape and fractured in LN2 (liquid nitrogen).

2.3. Positron Annihilation Lifetime Spectroscopy

A detailed description of the positron measurement apparatus and the method of analysis can be found in Ref. [11]. In short, the PALS experiments were carried out using a fast-fast coincidence lifetime setup (260 ps time resolution). The positron source was ^{22}Na deposited between two Kapton foils with thickness 7 μm. The source was sandwiched between two samples with dimensions 12 mm × 10 mm × 2 mm. Spectra were acquired with the samples kept in vacuum (10^{-5} Pa). Measurements were carried out at temperatures ranging between 183 and 323 K (uncertainty = ± 1 K) [11] and spectra were acquired at temperature intervals of 10 K. Each spectrum consists of approximately 3 × 10^6 annihilation events. The spectra were analyzed using PATFIT-88 routine analysis [18].

2.4. Gas permeation analysis

Gas transport measurements were carried out by gas phase permeation technique using membrane samples shaped in form of discs with thickness d between 0.2 and 0.3 mm. Fixed the sample temperature T, one side of the membrane (HPS: High Pressure Side) is exposed to the test gas kept at fixed pressure p_{HPS}. The other side (LPS: Low Pressure Side) faced a calibrated vacuum chamber of known volume V pumped to background pressures in the 10^{-7} mbar range. At time $t = 0$ a sectioning valve, separating the calibrated chamber from the pumping system, is closed. The gas permeates through the membrane and increases the pressure p_{LPS} that is measured as a function of time. After a transient time, which depends on the gas diffusivity and membrane thickness, the pressure $p_{LPS}(t)$ in the calibrated chamber linearly increases with time, indicating that the gas flow has assumed a constant value (stationary transport conditions). In stationary conditions the gas permeability P can be evaluated by the relation [19]:

$$P = \frac{V}{A} \frac{d}{RT_{cham}} \frac{1}{} \frac{dp_{LPS}(t)}{dt} \frac{1}{p_{HPS}} \tag{1}$$

where A is the membrane surface area, R the universal gas constant and T_{cham} the temperature of the calibrated chamber. Measurements were carried out at temperatures ranging from 313 to 373 K with p_{HPS} values between 2 × 10^4 and 8 × 10^4 Pa. Details on the experimental apparatus and procedures are presented in Refs. [11,19,20] and in references therein.

3. Results

3.1. Nanocomposites characterization

In Fig. 1 we present a SEM micrograph showing the morphology of the FLG nanoplatelets: it can be seen that filler particles have irregular polygonal shape with surface size ~10 μm. FLG platelets results slightly twisted and present a smooth surface. In Fig. 2 we show SEM micrographs of the samples' surface: Fig. 2(a) is pertinent to the pure epoxy membrane, while Fig. 2(b), (c) and (d), to the nanocomposites with 2.8, 4.3 and 5.7 vol % filler content, respec-tively. We can see that the pure epoxy sample presents a uniform, smooth morphology without structures or defects such as fractures or pinholes. The presence of fillers is evident observing the nano-composite surfaces: the FLG fillers can be distinguished in the subsurface polymer layers and result oriented with their surface parallel to the membrane surface. Fig. 3 is a typical example of the nanocomposite sample cross-section (in the inset we present the cross-section of the pure epoxy). In this figure we can clearly distinguish the filler particle uniformly surrounded by the polymer layers. The filler particle maintains its original shape and size as in Fig. 1 and appears oriented with its surface parallel to the mem-brane surface, as previously observed in the surface micrographs, see Fig. 2(b,c,d).

Fig. 4 shows the XRD spectra of the polymer nanocomposite membranes. In this figure, we only see the spectra pertinent to the samples with 2.8 and 5.7 vol % filler. Spectra show two intense peaks at 2θ ~26.6° and 2θ ~54.8° pertinent to the (0002) and (0004) reflection of the g-C structure: note that the intensity of the peaks increases with the filler content. The broad reflection peak at 2θ angles between ~10° and ~30° is due to the amorphous polymer matrix.

From these spectra the following information can be obtained:

i) The spectra of the nanocomposites only show (0002) lines of graphite [20,21] indicating that the surface of the FLG nano-platelets is parallel to surface of the membrane. Note that this result is in agreement with the orientation of the FLG fillers as revealed by the SEM micrographs in Fig. 2(b,c,d) and Fig. 3;

ii) the average thickness of the FLG nano-platelets w results to be 10 ± 1 nm as estimated by the analysis of the FWHM of the (0002) g-C line by the Debye-Scherrer equation;

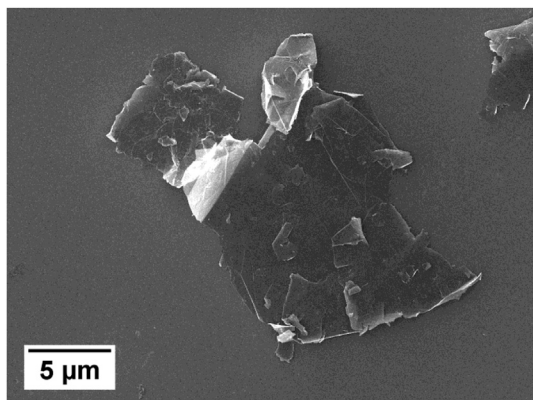iii) no ordered phase is induced in the matrix by the filler addition.

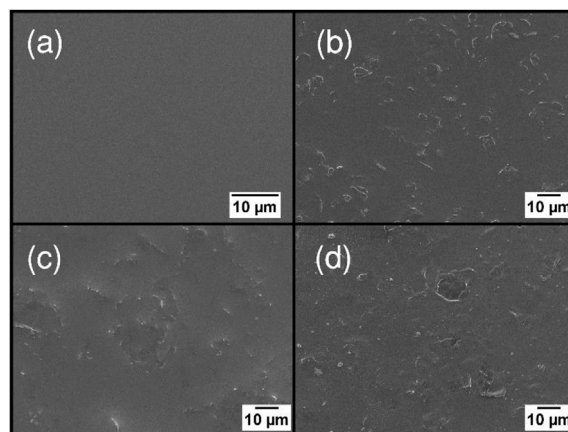**Fig. 1.** SEM micrograph of the as prepared FLG platelets.

Fig. 2. SEM micrograph of the pure epoxy membrane (a). Micrographs (b), (c) and (d) are pertinent to the nanocomposite membranes with 2.8, 4.3 and 5.7 vol % filler content, respectively.
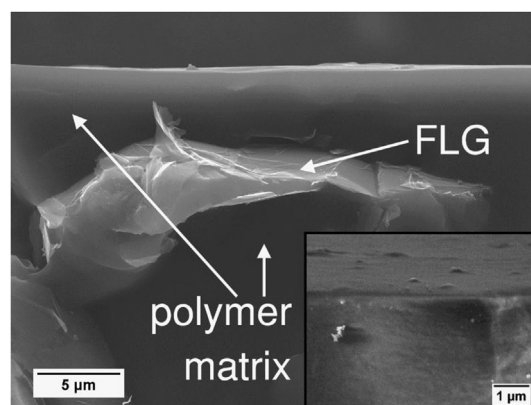
Fig. 3. Cross-section of the nanocomposite sample with 2.8 vol % FLG filler content. In the inset we report the cross-section of the pure epoxy. SEM images were taken after sample fracturing in liquid N$_2$.
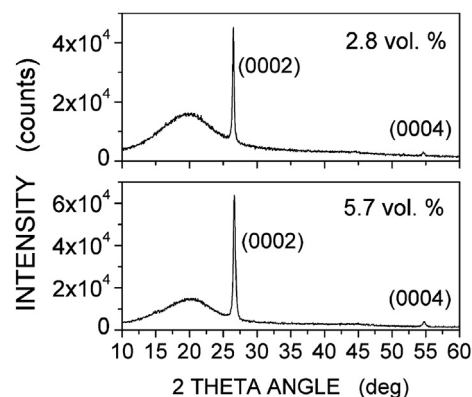
Fig. 4. XRD spectra of the polymer nanocomposites with 2.8 and 5.7 vol % FLG filler content.

3.2. Free volume structure

PALS spectra of the pure epoxy membrane were well fitted (chi-squared values laying between 1.01 and 1.11) by three discrete lifetime components $\tau_1 < \tau_2 < \tau_3$ with corresponding intensities I_1, I_2, I_3. Data fitting was done by fixing the *para*-positronium

lifetime τ_1 at 125 ns. The τ_2 value was found to increase from 0.344 ± 0.002 ns at 183 K to 0.399 ± 0.002 ns at 343 K [11]. PALS spectra pertinent to the nanocomposites were also well fitted with three lifetime components: (chi-squared values between 1.00 and 1.21). The obtained τ_2 values were found comparable with the values obtained in the pure membrane (from 0.335 ± 0.002 ns to 0.377 ± 0.002 ns for the sample with 5.7 vol % filler content). Fig. 5 shows the τ_3 values (right vertical axis) as a function of the sample temperature for the pure and for the nanocomposite samples. Assuming that free volume cavities have spherical shape, their average free volume v_h is given by the relation $v_h = 4\pi R^3/3$ where the average radius R can be calculated from the average value of τ_3 by the relation ($\Delta R = 0.166$ nm is the empirical electron-layer thickness [22,23]):

$$\tau_3 = \frac{1}{2}\left(1 - \frac{R}{R + \Delta R} + \frac{1}{2\pi}sin\left(\frac{2\pi R}{R + \Delta R}\right)\right)^{-1} \qquad (2)$$

The calculated values of v_h are reported in Fig. 5 on the left vertical axis. The variation of v_h with temperature can be split in two sections each well fitted with a straight line: the intersection of the two lines indicates the glass transition temperature T_g as seen by PALS analysis (see the vertical arrows). Note that the T_g value of the pure polymer, 229 ± 4 K [11], does not change after FLG filler addition. Differential Scanning Calorimetry (DSC) analyses, not reported here, confirm this result showing T_g values of 227 ± 2 K for all samples.

PALS data permits the analysis of the polymer free volume structure and the estimation of the fractional free volume f_h. The quantity $v_h I_3$ is, in fact, proportional to the fractional free volume f_h of the polymer [24,25].

The values of the o-Ps annihilation signal intensity (I_3) for the samples in rubbery state ($T > T_g$) are reported in Fig. 6.

A closer look at Figs. 5 and 6 shows that, at each of the examined temperatures ($T > T_g$), the v_h values obtained with the nanocomposite samples are almost equivalent to the v_h values obtained with the pure polymer matrix, while a progressive change of the I_3 parameter is observed with increasing filler content. The behavior of v_h and I_3 as a function of filler content shows that filler particles
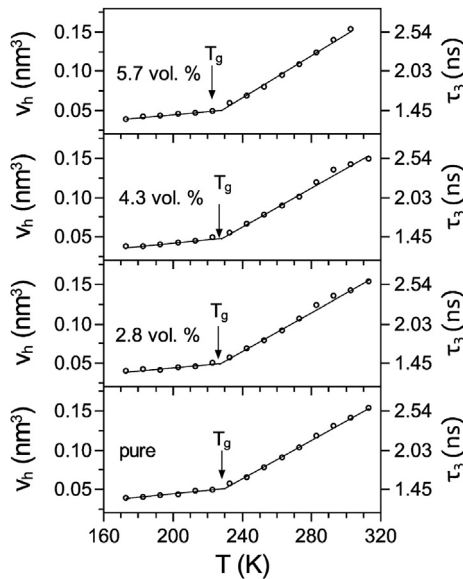

Fig. 6. Intensity of the o-Ps annihilation signal for the pure polymer matrix and for the nanocomposite samples in rubbery state ($T > T_g$).

don't change the free volume structure of the nanocomposite (i.e. v_h) but only reduce the number of the free volume holes. Hence, the variation of the fractional free volume, $f_v \propto v_h I_3$, in these nanocomposites is controlled by the variation of the intensity I_3.

Fig. 5. o-Ps lifetime values (τ_3, right vertical axis) and hole free volume (v_h, left vertical axis) as a function of the sample temperature for the pure polymer matrix (lower panel) and for the nanocomposite samples with different FLG filler content.
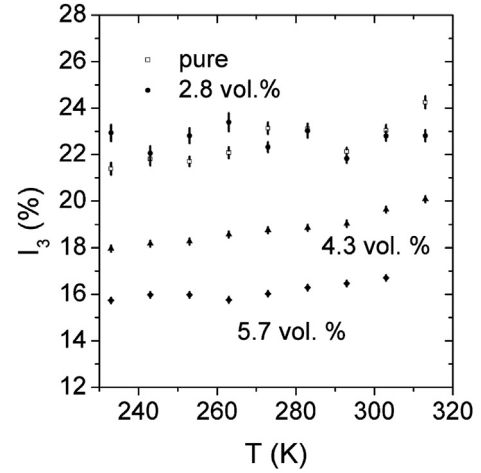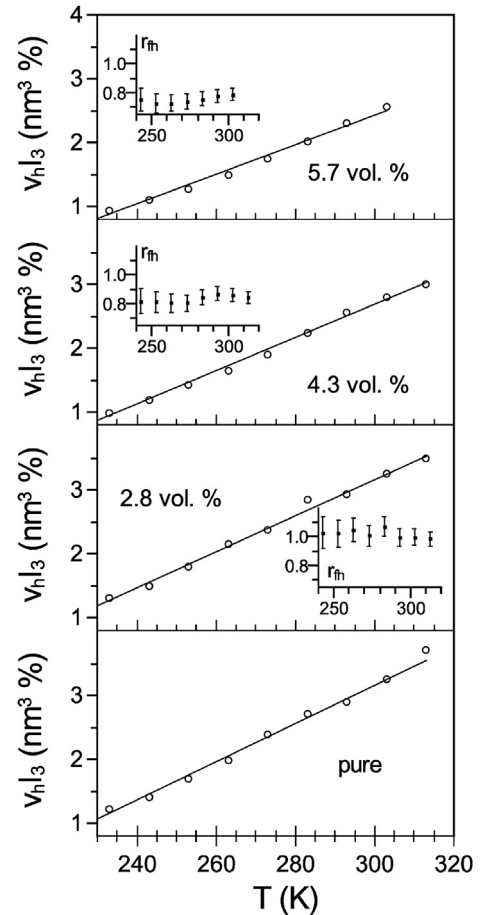

Fig. 7. $v_h I_3$ product (f_h is proportional to $v_h I_3$) as function of the temperature for the pure polymer matrix (lower panel) and the nanocomposite samples at $T > T_g$. Experimental errors are inside the symbols dimension. The solid line is a linear fit of the experimental points. The inset reports the ratio r_{fh} between the fractional free volume of the pure and of the nanocomposite samples (see text).

The $v_h I_3$ product as a function of the temperature for $T > T_g$ is shown in Fig. 7 $v_h I_3$ values are reported as symbols while the solid line is a linear fit. Experimental indeterminations in the $v_h I_3$ values are smaller than the size of the symbols. In the insets we report, for the nanocomposite samples, the ratio between the fractional free volume in the nanocomposites and the fractional free volume in the pure polymer membrane as taken on the fitting line:

$$r_{fh}(T) = f_h^{NC}/f_h^{pure} = (v_h I_3)_{NC}/(v_h I_3)_{pure}$$

Looking at the $r_{fh}(T)$ parameter we observe that: i) the filler addition introduces small changes of the fractional free volume f_h in the nanocomposite with 2.8 vol % filler while effectively reduces it in nanocomposites with 4.3 and 5.7 vol % filler, ii) for $T > T_g$ the free volume reduction parameter r_{fh} is almost constant with temperature.

It's worthy to point out that the reduction of the fractional free volume cannot be attributed only to the reduction of the polymer specific volume after the inclusion of the filler. Let us consider, for example, the nanocomposite sample with 4.3 vol % filler content. The inset of Fig. 7 shows that the fractional free volume is reduced by 14−15%. This reduction is thus at least three times larger than the reduction of the polymer specific volume.

3.3. Gas transport properties

In Fig. 8 we present the Arrhenius plot of the gases permeability values of the pure epoxy membrane P_C (C: continuous phase, open symbols) and of the nanocomposite membranes P_{NC} (NC: nanocomposite, solid symbols). Experimental values pertinent to the nanocomposite membrane with 0.6 vol % filler content are not presented because equivalent, inside the experimental indetermination, to those of the pure epoxy membrane. Experimental results indicate that the permeability of the nanocomposite membrane decreases with the filler addition for all examined gases. This decrease does not depend on the sample temperature and results comparable for the different test gases indicating that the filler addition does not introduce noticeable changes in the gas selectivity. The reduction of the gas permeability after filler addition to the polymer matrix can be quantitatively described by defining the $r_P^{exp} = P_{NC}/P_C$ parameter.

It can be observed that the permeability reduction does not depend on the nature of the gas and on the sample temperature. Accordingly to this finding, the values of r_P^{exp} for the test gases, as a function filler concentration, are reported in the insets of Fig. 8 for T = 334 K, only.

The measured gas permeability data were fitted by the relation $P = P_0 \exp\left(-\frac{E_P}{RT}\right)$ where R is the universal gas constant. Inside the experimental indetermination the values of the activation energy for permeation E_P don't vary with the filler content. The average E_P values for the nanocomposites are: $E_P (CO_2) = 5.0 \pm 0.2$ kcal/mol, $E_P (N_2) = 7.7 \pm 0.9$ kcal/mol and $E_P (H_2) = 7.6 \pm 0.6$ kcal/mol. These values are equivalent to those of the pure epoxy membrane: $E_P (CO_2) = 5.0 \pm 0.3$ kcal/mol, $E_P (N_2) = 8.7 \pm 0.5$ kcal/mol and $E_P (H_2) = 7.5 \pm 0.5$ kcal/mol [10]. The dispersion of the present FLG fillers in the epoxy layers improves the gas barrier properties of the membranes with effectiveness comparable to that observed with other graphene-based nanocomposites such as graphite nanoplatelets [6,20], graphene [26−28], functionalized graphene [29] or graphene oxide nanosheets [30] or with other high-aspect-ratio fillers such as silicate clays [31−33].

4. Discussion

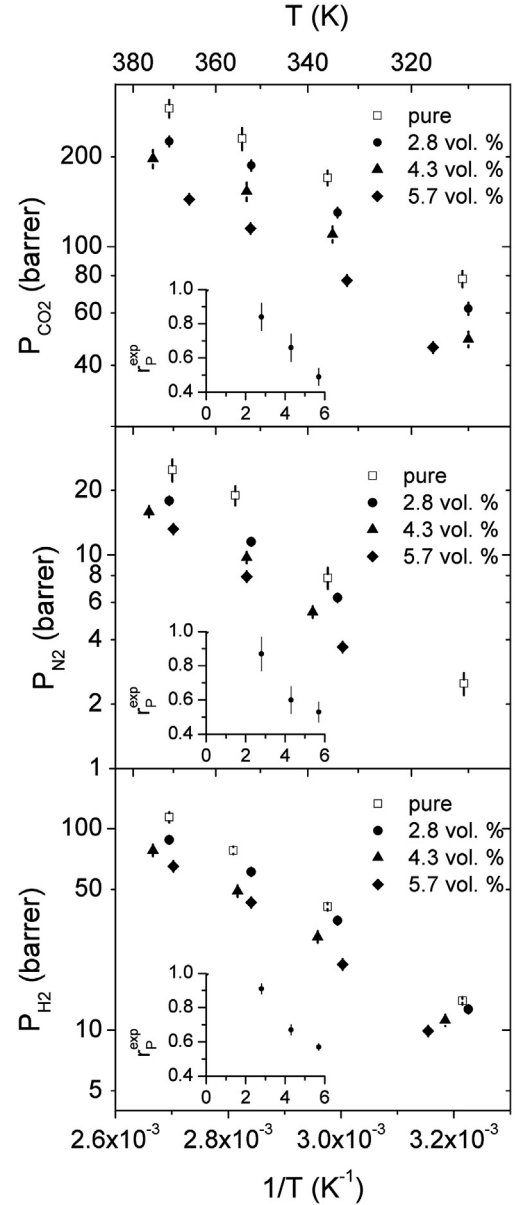The change in the gas permeability induced by the filler addition

Fig. 8. CO_2, N_2 and H_2 gas permeability values for the pure (P_C) and nanocomposite (P_{NC}) membranes. The insets of the figure report the $r_P^{exp} = P_{NC}/P_C$ parameter, as evaluated at T = 334 K (see section 3.3).

in the nanocomposites, see sect 3.3, will be here discussed in the framework of the permeation models for MMMs (Mixed Matrix Membranes), using the structural information on the nanocomposite samples presented in Sect. 3.1 and 3.2. To this task, we will analyze the $r_P^{exp} = P_{NC}/P_C$ parameter pertinent to the test gases at T = 334 K, which is shown in the insets of Fig. 8. We limit our attention to these data because, as discussed in section 3.3, r_P^{exp} was found not to depend on the sample temperature. Symbols in Fig. 9 represent the r_P^{exp} for the pure and nanocomposite membrane samples as a function of the filler content (expressed as volume fraction) for the examined test gases.

In an "ideal" nanocomposite the polymer phase completely wets the filler particles without changing the chemical-physical properties and the structure of the polymer matrix, including its gas permeability. When filler particles with permeability P_d form a dispersed phase with volume fraction ϕ_d in a continuous polymer matrix with permeability P_C then the transport properties of the
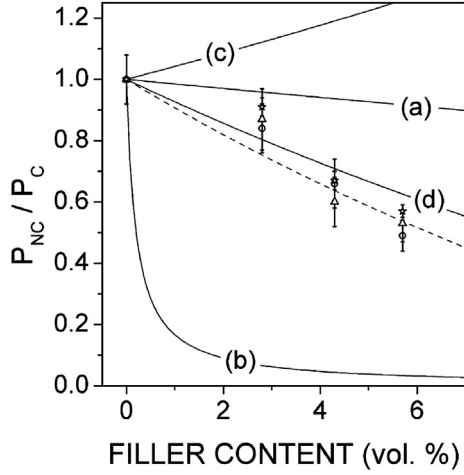
Fig. 9. Measured (symbols) and calculated (lines) P_{NC}/P_C values. Symbols represent the r_P^{exp} parameter at $T = 334$ K (circles: CO_2, stars: H_2, triangles: N_2). Line (a) is the calculated value of P_{NC}/P_C using the Maxwell equation, line (b) using the tortuous path model. Line (c) and (d) are calculated using the pseudo-dispersed phase model for the case of porous and rigidified interface layers, respectively. Line (d) was obtained with the experimentally obtained $l_{if} = 20$ nm value. The dashed line is also obtained assuming a rigidified interface layers but with $l_{if} = 25$ nm.

nanocomposite membrane P_{NC} can be predicted by two models [4,7–9]:

1. The first model is based on the Maxwell equation originally developed for the electrical conductivity of particulate composites [34] and describes the permeability P_{NC} of the nano-composite membrane by the following relation:

$$P_{NC}/P_C = \left[\frac{P_d + 2P_C - 2 \phi_d (P_C - P_d)}{P_d + 2P_C + \phi_d (P_C - P_d)} \right] \quad (3)$$

where ϕ_d is the filler volume fraction.

2. The second model, called "tortuous path" model predicts that the nanocomposite permeability is reduced by a factor τ (called "tortuosity factor"). Impermeable fillers, in fact, force gas molecules to go across a tortuous path with length λ larger than the membrane thickness d. For platelets with average thickness w and lateral size l which are iso-oriented with their surface normal to the direction of the permeation flux then $\lambda = \tau \times d$ and $\tau = \left(1 + \frac{l}{2w} \phi_d \right)$. Consequently:

$$P_{NC}/P_C = (1 - \phi_d)/\tau \quad (4)$$

Given the gas-impermeable nature of the present filler nanoparticles ($P_d = 0$) and using the experimental geometrical dimensions for the FLG reported in section 3.1, $w = 10$ nm and $l = 10 \times 10^{-6}$ m, the ratio P_{NC}/P_C can be calculated as function of the filler content. The solid lines (a) and (b) in Fig. 9 represent the P_{NC}/P_C values, as obtained by Maxwell model, eq. (3), and by the tortuous path model, eq. (4), respectively. The comparison between theoretical evaluation and experimental data indicates that the Maxwell qualitatively describes the linear decreasing trend of the r_P^{exp} parameter with the filler concentration but underestimates the experimentally observed reduction. The tortuous path model does not describe this trend and strongly overestimates the reduction of r_P^{exp} for any of the examined filler concentrations.

The failure of the previous model in describing the permeability reduction indicates that the gas transport properties of the present nanocomposite membranes depend on structural variations of the polymer matrix induced by the filler addition. The results of PALS analysis in section 3.2 point out that the filler addition gives rise to a sensible reduction of the fractional free volume of the nanocomposites compared to that of the pure polymer matrix.

In general, the contact between filler particles and polymer matrix is "non-ideal" because of the different chemical-physical properties of the two phases. De-wetting of the polymer chains from the filler surface often occurs and results in void spaces between filler and matrix. On the other hand, polymer chains in contact with the filler surface present different chain packing than in the matrix and thus a different free volume structure. In consequence of void formation or variation of the chain packing, the gas permeability of the polymer layers surrounding the filler particles results significantly different from the gas permeability of the matrix. In this case the gas transport properties of the nanocomposite can be modeled assuming that interfacial regions and filler particles form a pseudo-dispersed phase with effective permeability P_{ps} given by Refs. [4,7–9]:

$$P_{ps} = P_{if} \left[\frac{P_d + 2P_{if} - 2 \phi_s \left(P_{if} - P_d \right)}{P_d + 2P_{if} + \phi_s \left(P_{if} - P_d \right)} \right] \quad (5)$$

where P_{if} and ϕ_{if} are gas permeability and volume fraction of the interfacial layers while $\phi_s = \phi_d/(\phi_d + \phi_{if})$ is the volume fraction of the filler particle within the pseudo-dispersed phase [4,7–9]. When filler particles are thin sheets of thickness w, as in the present nanocomposites, and the interfacial region consists of a layer of thickness l_{if} formed on both surfaces of the filler particle, then ϕ_s can be calculated by the following equation [19]:

$$\phi_s = \phi_d \left/ \left(\phi_d + \phi_{if} \right) \right. = w \left/ \left(w + 2l_{if} \right) \right. \quad (6)$$

Polymer matrix and pseudo-dispersed phase form an idealized two-phase system where the pseudo-dispersed phase occupies a volume fraction $\phi_d + \phi_{if}$ and the permeability ratio P_{NC}/P_C can be evaluated by the following equation:

$$P_{NC}/P_C = \left[\frac{P_{ps} + 2P_C - 2 \left(\phi_d + \phi_{if} \right) (P_C - P_{ps})}{P_{ps} + 2P_C + \left(\phi_d + \phi_{if} \right) (P_C - P_{ps})} \right] \quad (7)$$

The required input parameters for the pseudo-dispersed phase model are the interface permeability P_{if} and the thickness l_{if} of the interfacial region.

The presence of interfacial voids always increases the gas permeability of the nanocomposites and cannot explain the observed decrease. The permeability P_{ps} of the interfacial regions in presence of voids can be roughly estimated as the Knudsen diffusivity $D_K = \frac{1}{3} d_{pore} \left(\frac{8 RT}{\pi M} \right)^{1/2}$ of the gas molecule in the nano-voids times their sorption coefficient $S_{void} = 1/R T$ [4,7–9]. Line (c) in Fig. 9 was obtained by eqs. (5)–(7) with $w = 10$ nm and $P_d = 0$, for the case of CO_2 as penetrant molecule with $d_{pore} = (6v_h/\pi)^{1/3} = 0.7$ nm, and $l_{if} = 3d_{pore}$. As expected from the above discussion, line (c) shows the opposite trend respect to that experimentally observed. Note also that the presence of voids at the filler-matrix interface can be excluded looking at PALS data. In fact, these voids and their internal surfaces would give rise to an increase of the o-Ps formation and thus its annihilation signal I_3 should increase with the filler content: this behavior is the opposite to that shown by the PALS spectra of the present nanocomposites.

Differently from voids at the interfaces, changes in the chain

packing of the polymer interfacial layers and the consequent free volume reduction give rise to the rigidification of the interface polymer layers that decreases the overall gas permeability [35,36]. The gas permeability of the interface regions P_{if} is lower than the gas permeability of the pure matrix by a factor β called "chain rigidification factor" ($P_{if} = P_C/\beta$).

To examine if rigidification effects quantitatively explain the reduction of the nanocomposite permeability using eqs. (5)–(7) we have simply modeled the nanocomposite as consisting of filler particles surrounded by a polymer domain which has the same geometry as the filler, see Fig. 10. The thickness h of this polymer region (above and below the filler) is fixed given the filler thickness w and the volume fraction. For $w = 10$ nm, see section 3.1, h values are 178, 120 and 88 nm for the nanocomposites with 2.8, 4.3 and 5.7 vol % FLG content, respectively. A fraction of this region, that is a layer of thickness $l_{if} = (1 - \alpha_r) h$ with $\alpha_r < 1$ at the polymer-filler interface, consists of rigidified polymer chains. Each polymer domain of volume $V = 2 L^2 h$ surrounding the filler particle can be thus divided into a rigidified sub-domain of volume $V_{if} = 2 L^2 l_{if} = 2 L^2 h(1 - \alpha_r)$ and a bulk-like sub-domain of volume $V - V_{if}$ where the polymer layers maintain the same properties as in the pure matrix.

To evaluate l_{if} we have assumed that the fractional free volume reduction in the present nanocomposites mainly occurs in these sub-domains at the filler-matrix interface. In fact, the following argument shows that the fractional free volume reduction cannot occur uniformly in the polymer matrix. Let us consider the relation between gas permeability P and fractional free volume f_h:

$$P = A_p \exp\left(-\frac{B_P}{f_h} \right) \tag{8}$$

where A_p and B_P are empirical parameters which depends on the size and shape of the penetrant molecules [37]. The observed 15–20% reduction of the fractional free volume, see insets of Fig. 4, when uniformly distributed in the polymer, would reduce the gas permeability of the nanocomposites more than what experimentally observed.

The l_{if} parameter can be thus experimentally evaluated using PALS data by the ratio $r_{fh}(T)$

$$\frac{V - V_{if}}{V} = \alpha_r = \frac{f_h^{NC}}{f_h^C} = r_{fh}(T) \tag{9}$$

The r_{fh} values reported in the insets of Fig. 4 permit to evaluate the values of the l_{if} parameter. For the nanocomposite with 4.3 and 5.7 vol % filler content $l_{if} = 18 \pm 4$ and $l_{if} = 20 \pm 3$ nm values are evaluated, respectively. The r_{fh} values for the 2.8 vol % nanocomposite inside the indetermination are similar to those of the pure sample and a meaningful l_{if} value cannot be obtained.
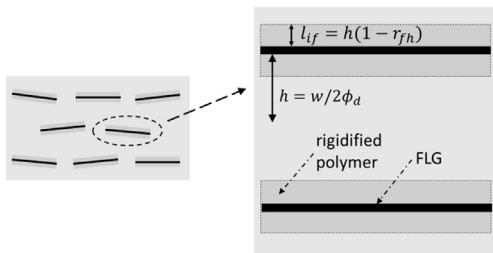

Fig. 10. Schematic picture of the polymer nanocomposites. Black rectangles: FLG filler nanoparticles (thickness w). Dark gray: rigidified polymer region at the filler-matrix interface. Light gray: unconstrained region of the polymer matrix. $2h$ is the average distance between FLG nano-platelets and l_{if} the thickness of the rigidified region.

On the other hand, if we now consider that the observed 15–20% free volume reduction is localized in this very thin interface region it is reasonable to assume, as a first hypothesis, that here a nearly complete polymer chain rigidification, occurs, that is $\beta = \infty$.

The complete rigidification of the polymer interface layers makes the interface layers gas impermeable, $P_{if} = 0$, and consequently $P_{ps} = 0$, see eq. (5). The permeation ratio in Eq. (6) reduces to:

$$P_{NC}/P_C = \frac{1 - \left(\phi_d + \phi_{if} \right)}{1 + \frac{1}{2}\left(\phi_d + \phi_{if} \right)} \tag{10}$$

and can be evaluated by using the obtained values of l_{if}. Considering FLG fillers of size l and thickness w surrounded by a rigidified layer of thickness l_{if} above and below the filler surface then (see Fig. 10):

$$\phi_d + \phi_{if} = \phi_d \left(1 + \frac{2l_{if}}{w} \right) \tag{11}$$

Line (d) in Fig. 9 was obtained by eqs. (10) and (11), using for l_{if} the value of 20 ± 3 nm, as experimentally obtained by PALS analysis with the 5.7 vol % filled nanocomposites. This line shows a good agreement with the experimental data and indicates that the permeability reduction in the nanocomposite samples can be attributed to the formation of a rigidified polymer region at filler-matrix interface. We also remark that data fitting weakly depends on the value of the chain rigidification factor once the value of l_{if} is fixed: in fact, assuming $\beta = 5$, then the P_{NC}/P_C values are less than 10% different from the values obtained with $\beta = \infty$. Note that similar remarks on the rigidification factor sensitivity were done also by other researchers [38–40].

From Fig. 9 it appears that PALS analysis slightly underestimates the thickness l_{if} of this rigidified region. In fact, a better accord between experimental data and eq. (7) can be obtained using $l_{if} = 25$ nm, see the dashed line in Fig. 9. This underestimation means that the free volume probed by positrons is slightly more than the free volume accessible to the penetrant molecules. It can be argued that the rigidified region reasonably contains free volume elements probed by positrons that are not accessible to gas molecules and don't contribute to their transport.

To complete this discussion, it is worthy to indicate that Maurer et al. in a PALS study of polymer nanocomposites containing graphene oxide fillers attributed the reduction of the I_3 signal to the presence of so-called "scavenger groups", that is electron-attracting moieties such as hydroxyl groups located at the surface of the filler particles [41]. The mechanism behind this effect was originally suggested by Eldrup et al. to explain the inhibition of Ps formation in water solutions containing positive ions [42]. Briefly, in the spur model, Ps forms with a spur electron at the end of the positron track upon e^+ slowing down [15,16]: according to Eldrup et al., ions in water solutions reduce the Ps formation yield, and thus the I_3 signal intensity, because they deplete the Ps-forming electrons from the spurs. In the system studied by Eldrup et al. this effect was effec-tively working because the diffusion length of the Ps forming spur electrons, estimated few nanometers, was close to the average distance between the ions [42]. This mechanism cannot explain the reduction of the I_3 signal intensity observed in the present FLG nanocomposite sample. Considering that freed electrons in polymers have a path of 1–3 nm [43–46], only electrons in the positron spurs that end less than 1–3 nm from the filler surface could be scavenged from positive groups here possibly present. This process would define a "*Ps-formation inhibited*" region surrounding the

filler particles with thickness of 1−3 nm which cannot account for the reduction of I_3 signal observed in the present nanocomposites. Possible defects of the filler particles (such as vacancies or vacancy clusters) or defects at their surface act as annihilation sites for thermalized positrons reaching them and give rise to an annihilation signal contributing to the τ_2 and I_2 components of the PALS spectra [47].

Finally, although the rigidification depends on the type of matrix and filler coupling, it is worth to compare the values of the l_{if} parameter obtained by the present PALS analysis with values reported in literature for polymer nanocomposites with similar filler high-aspect-ratio [48]. Studies on solvent uptake in poly(-etherimide)/montmorillonite nanocomposites indicates that the large uptake reduction at 5 wt % filler content is compatible with a thickness of the rigidified region close to 25 nm [49]. Measurements of the thickness of the constrained region was done by Adame et al. by Atomic Force Microscope in polyamide/clay nanocomposites analyzing the sample morphology: the authors reported that the rigidified layer extends approximately 40−50 nm far from the filler surface [50].

The formation of this rigidified layer does not change the T_g value of the nanocomposite samples, as it is seen by PALS, see Fig. 5. PALS analyses are based, in fact, on the $o\text{-}Ps$ formation and annihilation into free volume cavities, which do not form in this rigidified region.

In the present nanocomposite samples DSC analysis also shows that T_g does not change after filler addition. Negligible or no T_g variations are reported in literature in several nanocomposite samples [51−59]. As explained by Moll et al. [52] and by Indrakanti et al. [60] this behavior occurs when the interface layer is decoupled from the remaining part of the polymer matrix and does not relax in the timeframe of the DSC experiments. Consequently, the glass transition temperature is that of the remaining part of the polymer and does not change [52,60].

5. Conclusions

We have found that the gas permeability of the present polymer membranes decreases with the addition of FLG filler nanoparticles as consequence of the formation of a rigidified polymer regions surrounding the filler. The permeability decrease can be quantitatively described assuming that this region consists of gas-impermeable polymer layers and extend, in the present nanocomposites, from the filler surface for a thickness l_{if}. PALS data permits to quantitatively evaluate the l_{if} value, ~ 20 nm, by measuring the fractional free volume of the nanocomposite and its reduction with respect to that of the pure polymer matrix. In the present epoxy-FLG system the l_{if} value is in good accord with the values reported in literature for other polymer nanocomposite systems although evaluated with different experimental approaches.

Acknowledgements

References

[1] D.R. Paul, L.M. Robeson, Polymer nanotechnology: nanocomposites, Polymer 49 (2008) 3187−3204.

[2] Y. Cui, S.I. Kundalwal, S. Kumar, Gas barrier performance of graphene/polymer nanocomposites, Carbon 98 (2016) 313−333.

[3] H. Kim, A.A. Abdala, C.W. Macosko, Graphene/polymer nanocomposites, Macromolecules 43 (2010) 6515−6530.

[4] R. Pal, Permeation models for mixed matrix membranes, J. Colloid Interface Sci. 317 (2008) 191−198.

[5] E.L. Nielsen, Models for the permeability of filled polymer systems, J. Macromol. Sci. Part Pure Appl. Chem. 1 (1967) 929−942.

[6] K. Kalaitzidou, H. Fukushima, L.T. Drzal, Multifunctional polypropylene composites produced by incorporation of exfoliated graphite nanoplatelets, Carbon 45 (2007) 1446−1452.

[7] M.A. Aroon, M. Ismail, T. Matsuura, M.M. Montazer-Rahmati, Performance studies of mixed matrix membranes for gas separation: a review, Sep. Purif. Technol. 75 (2010) 229−242.

[8] T.T. Moore, W.J. Koros, Non-ideal effects in organic-inorganic materials for gas separation membranes, J. Mol. Struct. 739 (2005) 87−98.

[9] M. Rezakazemi, A. Ebadi Amooghin, M.M. Montazer-Rahmati, A.F. Ismail, T. Matsuura, State-of-the-art membrane based CO2 separation using mixed matrix membranes (MMMs): an overview on current status and future directions, Prog. Polym. Sci. 39 (2014) 817−861.

[10] P.N. Patil, D. Roilo, R.S. Brusa, A. Miotello, R. Checchetto, Influence of nano-level molecular packing on the gas transport properties in amine-modified epoxy resins, Polymer 58 (2015) 130−138.

[11] P.N. Patil, D. Roilo, R.S. Brusa, A. Miotello, S. Aghion, R. Ferragut, R. Checchetto, Free volumes and gas transport in polymers: amine-modified epoxy resins as a case study, Phys. Chem. Chem. Phys. 18 (2016) 3817−3824.

[12] G. Chen, D. Wu, W. Weng, C. Wu, Exfoliation of graphite flake and its nanocomposites, Carbon 3 (2003) 619−621.

[13] B.M. Yoo, H.J. Shin, H.W. Yoon, H.B. Park, Graphene and graphene oxide and their uses in barrier polymers, J. Appl. Polym. Sci. 131 (2014) 39628.

[14] J.R. Potts, D.R. Dreyer, C.W. Bielawski, R.S. Ruoff, Graphene-based polymer nanocomposites, Polymer 52 (2011) 5−25.

[15] P.E. Mallon, Application to polymers, in: P.E. Mallon, Y.C. Jean, D.M. Schrader (Eds.), Princ. Appl. Positron Positronium Chem, World Scientific, Singapore, 2003, pp. 253−280.

[16] G. Consolati, F. Quasso, Morphology of free-volume holes in amorphous polymers by means of positron annihilation lifetime spectroscopy, in: L.A. Utracki, A.M. Jamieson (Eds.), Polym. Phys. Suspens. Nanocomposites beyond, John Wiley and Sons, Hoboken, 2010, pp. 393−420.

[17] G. Carotenuto, S. De Nicola, G. Ausanio, D. Massarotti, L. Nicolais, G.P. Pepe, Synthesis and characterization of electrically conductive polyethylene supported graphene films, Nanoscale Res. Lett. 9 (2014) 475.

[18] P. Kirkegaard, N.J. Pedersen, M. Eldrup, PATFIT-88, Risoe Natl. Lab. Rosk. Den. (1989). Series: Risø-M No. 2740.

[19] R. Checchetto, N. Bazzanella, B. Patton, A. Miotello, Palladium membranes prepared by r.f. magnetron sputtering for hydrogen purification, Surf. Coat. Technol. 177−178 (2004) 73−79.

[20] R. Checchetto, A. Miotello, L. Nicolais, G. Carotenuto, Gas transport through nanocomposite membrane composed by polyethylene with dispersed graphite nanoplatelets, J. Membr. Sci. 463 (2014) 196−204.

[21] S. Dimovski, A. Nikitin, H. Ye, Y. Gogotsi, Synthesis of graphite by chlorination of iron carbide at moderate temperatures, J. Mat. Chem. 14 (2004) 238−243.

[22] S.J. Tao, Positronium annihilation in molecular substances, J. Chem. Phys. 56 (1972) 5499−5510.

[23] M. Eldrup, D. Lightbody, J.N. Sherwood, The temperature dependence of positron lifetimes in solid pivalic acid, Chem. Phys. 63 (1981) 51−58.

[24] J. Krištiak, J. Bartoš, K. Krištiaková, O. Šauša, P. Bandžuch, Free-volume microstructure of amorphous polycarbonate at low temperatures determined by positron-annihilation-lifetime spectroscopy, Phys. Rev. B 49 (1994) 6601−6607.

[25] Y.C. Jean, J.D. Van Horn, W.-S. Hung, K.-R. Lee, Perspective of positron annihilation spectroscopy in polymers, Macromolecules 46 (2013) 7133−7145.

[26] O.C. Compton, S. Kim, C. Pierre, J.M. Torkelson, S.T. Nguyen, Crumpled graphene nanosheets as highly effective barrier property enhancers, Adv. Mater 22 (2010) 4759−4763.

[27] K.K. Sadasivuni, A. Saiter, N. Gautier, S. Thomas, Y. Grohens, Effect of molecular interactions on the performance of poly(isobutylene-co-isoprene)/graphene and clay nanocomposites, Colloid Polym. Sci. 291 (2013) 1729−1740.

[28] J. Jin, R. Rafiq, Y.Q. Gill, M. Song, Preparation and characterization of high performance of graphene/nylon nanocomposites, Eur. Polym. J. 49 (2013) 2617−2626.

[29] H. Kim, C.W. Macosko, Processing-property relationships of polycarbonate/graphene composites, Polymer 50 (2009) 3797−3809.

[30] J. Wu, G. Huang, H. Li, S. Wu, Y. Liu, J. Zheng, Enhanced mechanical and gas barrier properties of rubber nanocomposites with surface functionalized graphene oxide at low content, Polymer 54 (2013) 1930−1937.

[31] J.M. Herrera-Alonso, Z. Sedláková, E. Marand, Gas transport properties of polyacrylate/clay nanocomposites prepared via emulsion polymerization, J. Membr. Sci. 363 (2010) 48−56.

[32] M.A. Osman, V. Mittal, M. Morbidelli, U.W. Suter, Epoxy-layered silicate nanocomposites and their gas permeation properties, Macromolecules 37 (2004) 7250−7257.

[33] Y. Cui, S. Kumar, B.R. Kona, D. van Houcke, Gas barrier properties of polymer/clay nanocomposites, RSC Adv. 5 (2015) 63669−63690.

[34] J.C. Maxwell, A Treatise on Electricity and Magnetism, Oxford Univ. Press,

London, 1873.

[35] S. Kim, E. Marand, J. Ida, V.V. Guliants, Polysulfone and mesoporous molecular sieve MCM-48 mixed matrix membranes for gas separation, Chem. Mater 18 (2006) 1149−1155.

[36] R. Mahajan, W.J. Koros, Mixed matrix membrane materials with glassy polymers. Part 1, Polym. Eng. Sci. 42 (2002) 1420−1431.

[37] S. Matteucci, Y. Yampolskii, B.D. Freeman, I. Pinnau, Transport of gases and vapors in glassy and rubbery polymers, in: Y. Yampolskii, I. Pinnau, B.D. Freeman (Eds.), Mater. Sci. Membr. Gas Vap. Sep, John Wiley & Sons, Ltd, Chichester, West Sussex, England, 2006, pp. 1−48.

[38] R. Mahajan, Formation, Characterization and Modeling of Mixed Matrix Membranes Materials, Ph. D. dissertation, The University of Texas, 1998.

[39] Y. Li, T.S. Chung, C. Cao, S. Kulprathipanja, The effects of polymer chain rigidification, zeolite pore size and pore blockage on polyethersulfone (PES)-zeolite A mixed matrix membranes, J. Membr. Sci. 260 (2005) 45−55.

[40] T.T. Moore, R. Mahajan, D.Q. Vu, W.J. Koros, Hybrid membrane materials comprising organic polymers with rigid dispersed phases, AIChE J. 50 (2004) 311−321.

[41] F.H. Maurer, C.R. Arza, Dispersion and interaction of graphene oxide in amorphous and semi-crystalline nano-composites: a PALS study, in: J. Phys. Conf. Ser, IOP Publishing, 2015, p. 012020.

[42] M. Eldrup, V.P. Shantarovich, O.E. Mogensen, Inhibition of Ps formation by strong Ps quenchers, Chem. Phys. 11 (1975) 129−142.

[43] S.M. Pimblott, J.A. LaVerne, A. AlbaGarcia, L.D. Siebbeles, Energy loss by nonrelativistic electrons and positrons in polymers and simple solid hydrocarbons, J. Phys. Chem. B 104 (2000) 9607−9614.

[44] Y. Tanaka, N. Ohnuma, K. Katsunami, Y. Ohki, Effects of crystallinity and electron mean-free-path on dielectric strength of low-density polyethylene, IEEE Trans. Electr. Insul. 26 (1991) 258−265.

[45] P. de Vera, I. Abril, R. Garcia-Molina, Inelastic scattering of electron and light ion beams in organic polymers, J. Appl. Phys. 109 (2011) 094901.

[46] M. Dapor, A comparative study of electron and positron penetration in silicon dioxide, J. Electron Spectrosc. Relat. Phenom. 151 (2006) 182−192.

[47] Z. Tang, M. Hasegawa, T. Shimamura, Y. Nagai, T. Chiba, Y. Kawazoe, M. Takenaka, E. Kuramoto, T. Iwata, Stable vacancy clusters in neutron-irradiated graphite: evidence for aggregations with a magic number, Phys. Rev. Lett. 82 (1999) 2532−2535.

[48] A. Gurses, Introduction to Polymer−Clay Nanocomposites, CRC Press, Boca Raton, 2015.

[49] M. Pramanik, H. Acharya, S.K. Srivastava, Exertion of inhibiting effect by aluminosilicate layers on swelling of solution blended EVA/clay nanocomposite, Macromol. Mat. Eng. 289 (2004) 562−567.

[50] D. Adame, G.W. Beall, Direct measurement of the constrained polymer region in polyamide/clay nanocomposites and the implications for gas diffusion, Appl. Clay Sci. 42 (2009) 545−552.

[51] A. Bansal, H. Yang, C. Li, K. Cho, B. Benicawicz, S. Kumar, L. Schadler, Quantitative equivalence between polymer nano-composites and thin polymer films, Nat. Mater 4 (2005) 693−698.

[52] J. Moll, S.K. Kumar, Glass transitions in highly attractive highly filled polymer nanocomposites, Macromolecules 45 (2012) 1131−1135.

[53] S.E. Harton, S.K. Kumar, H. Yang, T. Koga, K. Hicks, H. Lee, J. Mijovic, M. Liu, R.S. Vallery, D.W. Gidley, Immobilized polymer layers on spherical nanoparticles, Macromolecules 43 (2010) 3415−3421.

[54] P. Rittigstein, J.M. Torkelson, Polymer−nanoparticle interfacial interactions in polymer nanocomposites: confinement effects on glass transition temperature and suppression of physical aging, J. Polym. Sci. Part B Polym. Phys. 44 (2006) 2935−2943.

[55] H. Lu, S. Nutt, Restricted relaxation in polymer nanocomposites near the glass transition, Macromolecules 36 (2003) 4010−4016.

[56] B.J. Ash, L.S. Schadler, R.W. Siegel, Glass transition behavior of alumina/poly-methylmethacrylate nanocomposites, Mat. Lett. 55 (2002) 83−87.

[57] A.P. Holt, P.J. Griffin, V. Bocharova, A.L. Agapov, A.E. Imel, M.D. Dadmun, J.R. Sangoro, A.P. Sokolov, Dynamics at the polymer/nanoparticle interface in poly(2-vinylpyridine)/silica nanocomposites, Macromolecules 47 (2014) 1837−1843.

[58] A.P. Holt, J.R. Sangoro, Y. Wang, A.L. Agapov, A.P. Sokolov, Chain and segmental dynamics of poly(2-vinylpyridine) nanocomposites, Macromolecules 46 (2013) 4168−4173.

[59] F.W. Starr, J.F. Douglas, D. Meng, S.K. Kumar, Bound layers "cloak" nanoparticles in strongly interacting polymer nanocomposites, ACS Nano 10 (2016) 10960−10965.

[60] A. Indrakanti, R.L. Jones, S.K. Kumar, Do "nonequilibrium" effects control strong surface segregation from polymer blends? Macromolecules 37 (2004) 9−12.